Platform for Remote, Multifocal Brain Interventions

***Taylor D. Webb[1], Matthew G. Wilson[1], Henrik Odéen[2], and Jan Kubanek[1]**

[1]Department of Biomedical Engineering, University of Utah
[2]Department of Radiology and Imaging Sciences, University of Utah

ABSTRACT

Transcranial focused ultrasound brings precision healthcare to the human brain, delivering focal interventions to deep brain sites without the need for surgeries or systemic drug administrations. The approaches have included neuromodulation and localized delivery of drugs through an intact or temporarily opened blood brain barrier. Clinical translation of these approaches requires a system that can deliver ultrasound into specific brain targets on command. Here, we demonstrate a platform with these features, and validate its function in nonhuman primates. Specifically, we used the system to flexibly modulate two deep brain nuclei—the left and right lateral geniculate nucleus–during visual choice behavior. We found that ultrasound induced a behavioral bias whose polarity depended on the stimulation waveform. Moreover, repeated applications of ultrasound over 39 consecutive behavioral sessions produced no signs of harm to the stimulated circuits. The system can be be applied to diagnose and possibly treat disorders of brain function with a precision and flexibility previously unattainable.

Introduction

Nearly one in four people lives with a significant neurological or psychiatric disorder[1,2], and approximately one in three of the patients does not respond to drugs or has intolerable side effects[3–8]. Neuromodulation could provide these people with new treatment options, but invasive, surgical methods do not provide the necessary flexibility and non-invasive methods do not have the necessary spatial resolution at depth. Thus, there is no tool that would allow us manipulate specific deep brain circuits in the human brain noninvasively and at high spatial precision. Transcranial focused ultrasound is an emerging technology capable of delivering such noninvasive treatments, using rapid electronic steering to manipulate one or more deep brain regions with millimeter and microsecond precision. Depending on stimulus duration, ultrasound modulates neural activity[9–14] or induces changes in functional connectivity[15–17]. In addition, when combined with nanoparticles or microbubbles, ultrasound can be used to deliver drugs, genes, or stem cells selectively into the specified target/s. This can be achieved by releasing drugs from nanoparticle carriers,[18–20] or using microbubbles to temporarily disrupt the blood brain barrier[21] and so deliver large agents that would not pass otherwise. Thus, this form of energy provides novel therapeutic options for the millions of patients who are currently not adequately treated.

However, these applications are limited by technological challenges. A key requirement for the success of the ultrasound-based therapies is the ability to target a specified site flexibly and reproducibly. This flexibility is critical given that the neural sources of many psychiatric and neurological disorders are poorly understood and vary from individual to individual[22–25]. Systems that could provide this functionality—phased arrays—are currently only designed for ablative treatments. However, ablative systems are expensive, require continuous MR-imaging[26] and are impractical for reversible therapies.

We developed a system that manipulates deep brain circuits remotely and programmatically, thus enabling routine circuit manipulations in the clinics and research settings. The platform enables an operator to specify one or more targets, together with the desired timing and ultrasonic waveform, in software.

The design is MR-compatible, which enables clinicians and researchers to confirm precise targeting. The system's imaging functionality ensures reproducible positioning of the device and evaluates the quality of the ultrasound coupling to a subject's head. We validated these capabilities in a nonhuman primates (NHP). The system can be used to validate existing and device new ultrasonic protocols in NHPs, other large animals, or humans. Ultimately, the system will be used to provide precision treatments to patients who are currently out of options.

Results

We developed a practical and affordable platform that delivers focused ultrasound into specified deep brain targets remotely, with the skull and skin intact (Figure 1, top). The targets of the ultrasound are specified in software. The software can flexibly target individual sites in sequence (Figure 1, bottom) or simultaneously.

We validated these features in NHPs. Specifically, we used the platform to programmatically deliver focused ultrasound of specific parameters into the left and right LGN while we assessed the effects of the ensuing neuromodulation on behavior (Figure 1, top).

We found that brief, 300 ms pulses of ultrasound directed into the left and right LGN transiently modulated choice behavior in a NHP. The animal was asked to look at a left or a right target, whichever appeared first. We quantified effects of the ultrasonic neuromodulation in the controlled condition in which both targets appeared at the same time. We assessed the proportion of choices of each target when the left LGN was stimulated, when the right LGN was stimulated, and quantified the proportion of choices of the contralateral target for these conditions. The resulting proportion of contralateral choices, averaged across individual sessions, is shown in (Figure 2).

We observed a double dissociation of the effect polarity with respect to stimulation waveform. Specifically, we found that stimuli pulsed at 10% duty cycle induced a significant (one-sided t-test, $t(11) = -2.72$; $p = 0.02$) ipsilateral bias, consistent with an inhibition or disruption of the neural activity in the target circuit. On the other hand, continuous stimuli induced a significant (one-sided t-test, $t(17) = 2.25$; $p = 0.038$) contralateral bias, consistent with an excitation of the neural activity within the LGN.

Notably, in this analysis, we only compared effects for trials in which there always was an ultrasound stimulus (either a left or the right LGN was sonicated). This controls for potential generic artifacts that can be associated with ultrasound[27,28]. In addition, we found a significant change in the subject's behavior as a function of the stimulus duty cycle (one-way ANOVA, $F(2,36) = 7.6$; $p = 0.002$;). This provides additional control. Notably, the stimulus that delivered 10 times less energy into the target (10% duty) produced a stronger effect compared to the more potent 100% duty stimulus. This corroborates the notion that duty cycle constitutes a critical variable in the neuromodulatory effects of ultrasound[29], and the growing consensus that the effects of low-intensity ultrasound are of mechanical, as opposed to thermal, nature[30–33]. An additional control is seen in the lateralized effects of sonicating the left and right LGN, which reverse as a function of duty cycle (Supplemental Figure 1).

We delivered the ultrasound into the deep brain targets repeatedly, over 39 sessions. This enabled us to test the long-term safety of repeated ultrasonic neuromodulation. Specifically, damage to the LGN would result in a decrease in the subject's accuracy. We found the opposite (Figure 3). The subject's discrimination accuracy kept increasing over the course of the study ($p < 10^{-5}$, line fit to the data in Figure 3). This result demonstrates that repeated ultrasonic neuromodulation in primates is safe.

Repeated delivery of ultrasound into the brain rests on reproducible positioning of the device and on good coupling of the transducer face to the subject's skin. To address these critical aspects of ultrasound delivery, we equipped the platform with imaging functionality that ensures reproducible positioning with

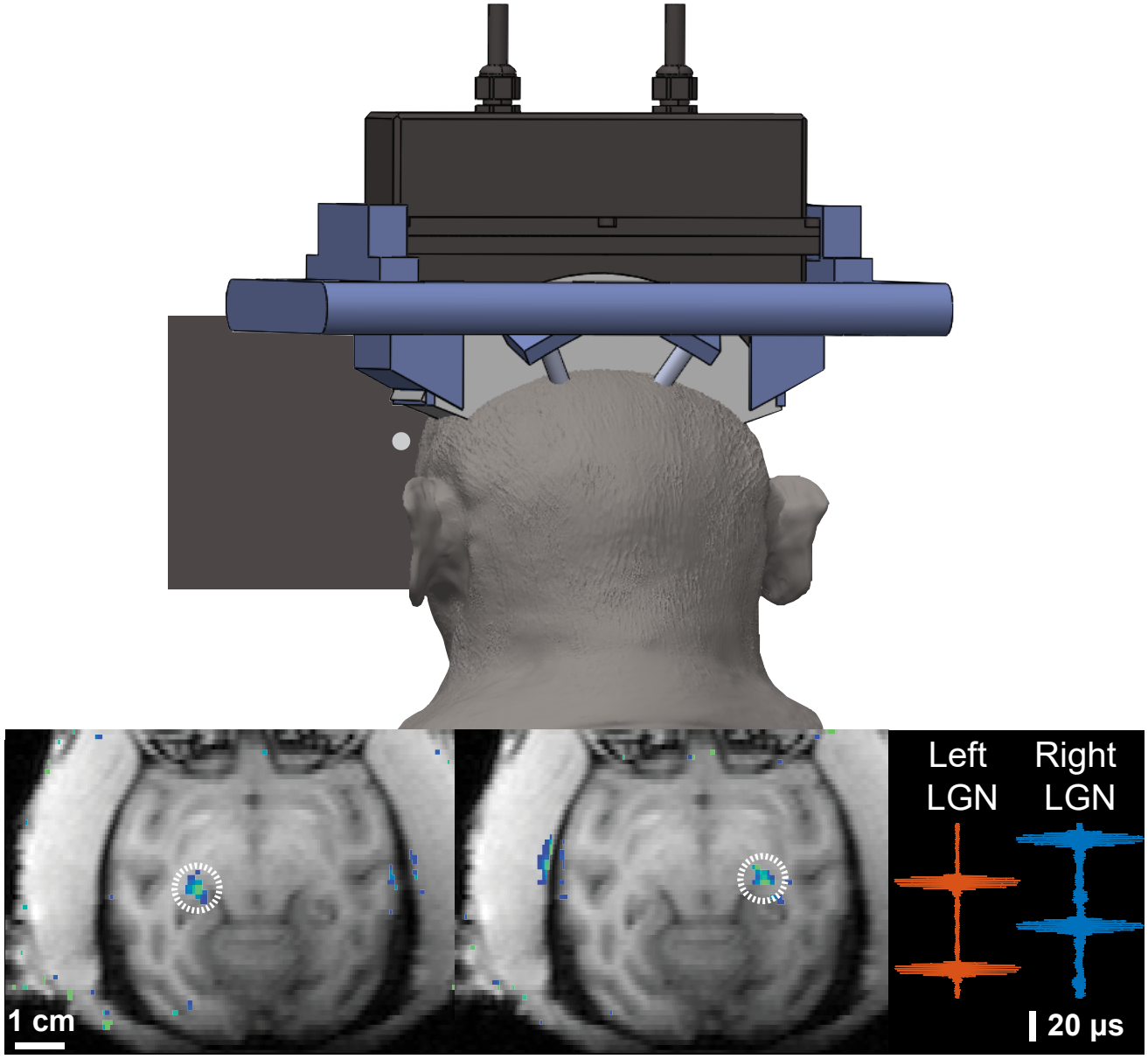

Figure 1. Platform for multifocal deep brain interventions.
Top: The platform is attached to the head of a NHP to provide reproducible targeting of deep brain circuits while the subject engages in behavioral tasks.
Bottom Left: Ultrasound targets are specified programmatically. This figure shows selective targeting of the left and right lateral geniculate nucleus (LGN). Image overlays were acquired using MRI thermometry (see Methods).
Bottom Right: The platform can be used to target multiple sites in rapid succession (minimum pulse separation of approximately 30 μs) or simultaneously. The figure shows acoustic traces simultaneously recorded by two hydrophones placed at the approximate location of the left and right LGN.

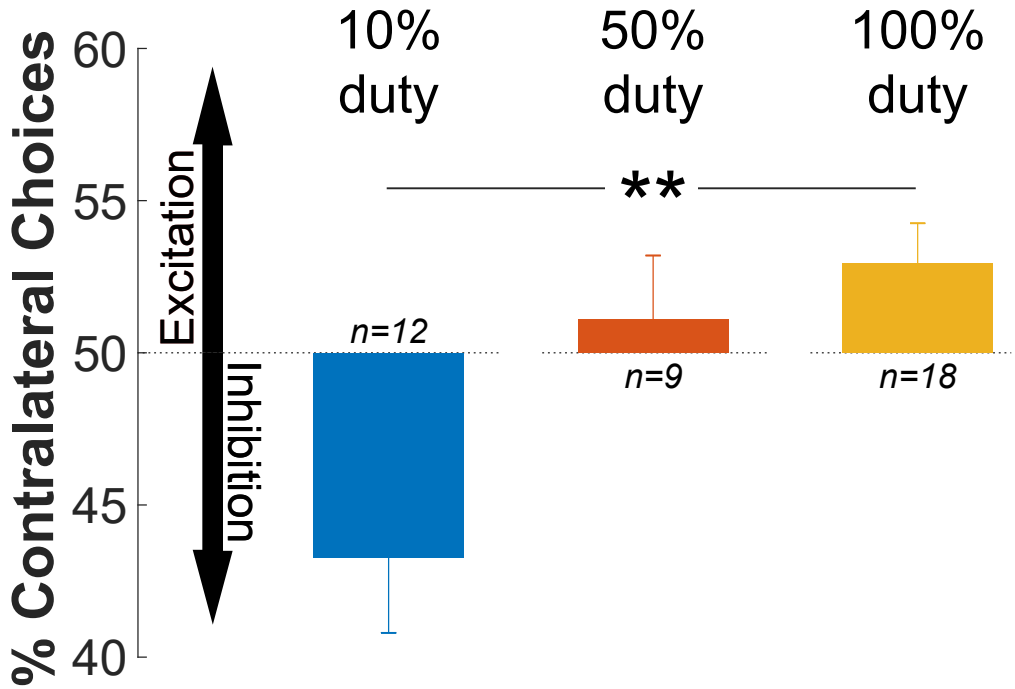

Figure 2. Selective excitation or inhibition of deep brain nuclei with immediate effects on choice behavior. Brief, low-intensity ultrasound (300 ms, 650 kHz, 750 kPa pressure at target) was delivered into the left or right LGN every 6-14 s. The side of the stimulation was randomized. The animal was deciding whether to look at a left or a right target. The brief, low-intensity ultrasonic pulses were able to change that choice proportion. Specifically, variation in the duty cycle of the ultrasound significantly changes the proportion of contralateral choices . Continuous stimuli signnificantly increased the proportion of contralateral choices whereas stimuli pulsed at 10% duty significantly decreased it. These effects are consistent with neuronal excitation and inhibition, respectively (vertical arrows). $**$: $p < 0.01$.

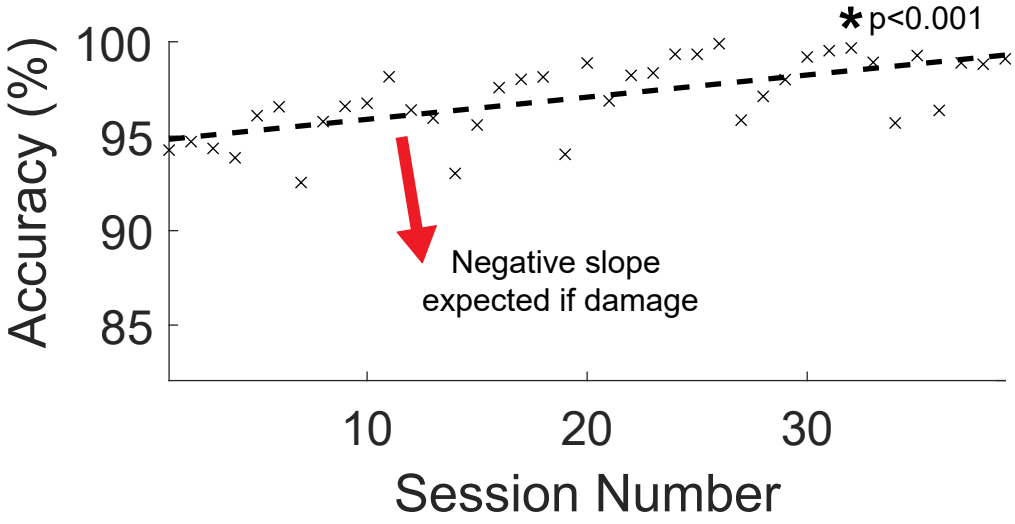

Figure 3. Repeated application of neuromodulatory ultrasound to deep brain circuits is safe. Damage to the LGN would cause a dramatic decline in the subject's visual discrimination performance, illustrated by the red arrow. We observe the opposite: the subject's discrimination accuracy improved from day to day. This demonstrates that the repeated neuromodulation was safe at the behavioral level. p: significance of slope term in linear fit.

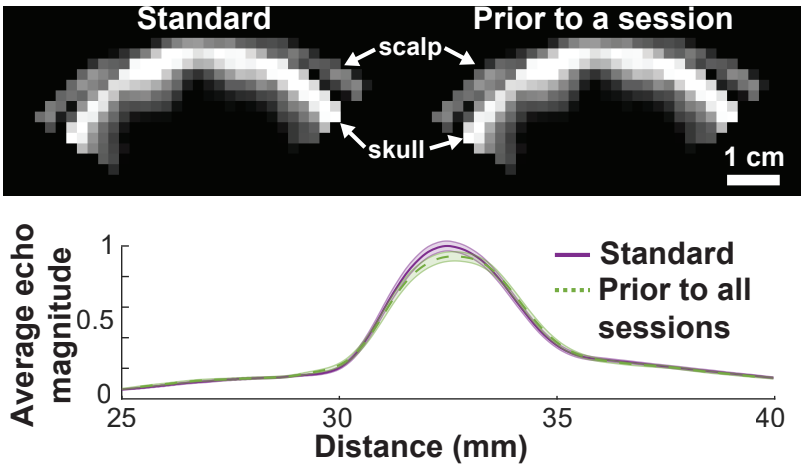

Figure 4. The system operated in imaging mode to ensure reproducible positioning and coupling. Prior to each session, the platform is operated in imaging mode. **Top:** The imaging reliably detects the location of the scalp and the skull. **Bottom:** The timing of the echoes received from the skull provide information on the position of the device with respect to the skull; their magnitude evaluates the quality of ultrasound coupling to the subject's head.

respect to the skull and quality coupling (Figure 4). Specifically, the device has a receive capability that also enables pulse-echo imaging. The ultrasound images acquired during each session are compared with a standard taken during an MRI imaging session that validated the targeting. This way, the operator can confirm an accurate placement of the array from session to session. In addition, the magnitude of the received echoes (Figure 4, bottom) provides information on the quality of the coupling.

Discussion

We developed and validated a practical and MRI-compatible platform that delivers ultrasound through the intact skull and skin into one or more neural targets in awake subjects. The platform unleashes the full potential of ultrasound: targeted noninvasive interventions deep in the brain (Figure 5). No other existing approach offers this desirable intersection of strengths.

Current clinical systems (e.g., ExAblate Neuro, Insightec[26]) are not designed for repeated, systematic applications in awake subjects. Emerging systems use single element transducers with poor axial resolution and without electronic focusing capabilities. Thus, these systems are unable to rapidly adjust the acoustic focus or target multiple sites at the same time or in concert. Moreover, none of these systems have imaging capabilities to validate the device's position with respect to the head and to test the quality of the ultrasound coupling. The platform described here was designed to fill these gaps and to power the novel treatments afforded by focused ultrasound. The programmatic targeting provides the sorely needed tool to flexibly target multiple neural structures, enabling clinicians to determine which neural circuits should be treated in each individual patient.

Figure 2 demonstrates that specific ultrasound waveforms can be harnessed for specific neuromodulation kinds (e.g., excitation and inhibition). This study provides first evidence that bi-polar neuromodulation of this kind is possible, within the same subject. This flexible, programmatic selection of the stimulation waveform is, besides the flexible targeting, a hallmark of ultrasound-based neuromodulation.

The effects shown in this study provide evidence that ultrasound modulates neuronal activity directly rather than through a confound. It has been suggested that the neuromodulatory effects of ultrasound might be due to an auditory artifact[27,28]. Our platform's fixed positioning and its capacity to programmatically

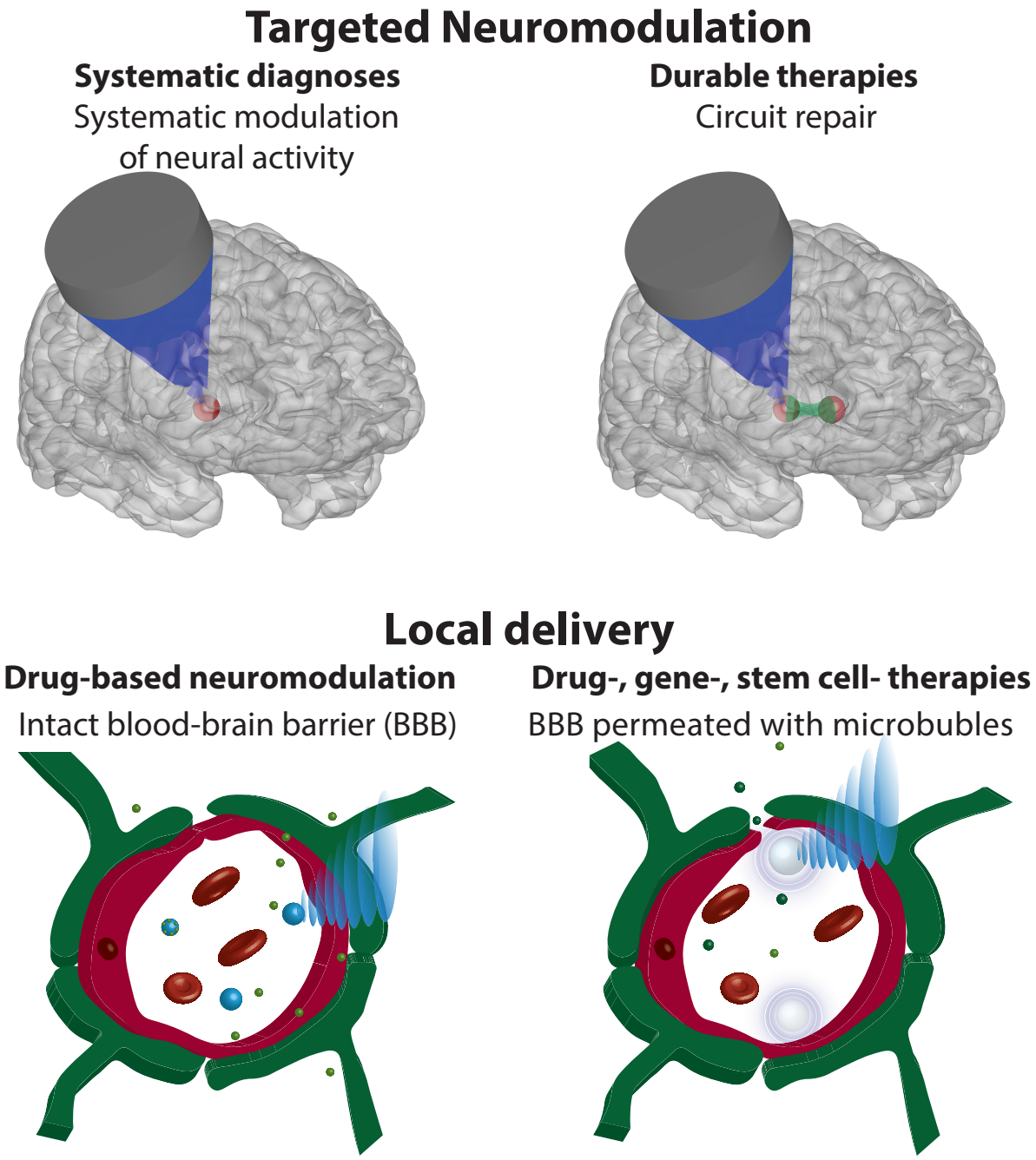

Figure 5. Applications of the platform for novel treatments of brain disorders.
Brief, millisecond-second ultrasound stimuli modulate neural activity in a transient fashion. This effect, when coupled with successive targeting of individual circuit candidates, provides a tool to dissect circuit function and dysfunction (top left). Ultrasound delivered into a target for minutes induces neuroplastic changes in the target. This could be used for durable reset of the malfunctioning circuits (top right). To further increase the specificity of these effects, ultrasound can be combined with drug-carrying nanoparticles that release their cargo specifically at the ultrasound target (bottom left). If agents that do not naturally cross the blood-brain barrier (BBB) are to be delivered into a target, ultrasound can be combined with microbbubles that—upon sonication—transiently permeate the BBB (bottom right).

test the effects of multiple sonication parameters on multiple deep brain targets enabled us to control for such artifacts. Specifically, if the effects described here were due to a generic artifact, there would be no specificity with respect to the stimulated LGN side, and no specificity with respect to the ultrasound waveform. Moreover, there could be no double dissociation of the effect polarity through the stimulation waveform (Figure 2, Supplemental Figure 1).

Future Applications

The manipulation of circuit function and dysfunction in the short term, as shown here, will be critical to future systematic and personalized diagnoses of the neural sources of brain disorders, and to basic investigations of brain function in humans. Moreover, the platform will enable researchers to deliver into the brain stimuli of substantial duration, and thus induce plastic reset[15–17] of the circuits diagnosed to be malfunctioning in each individual. The concept of the reset follows that of electroconvulsive therapy, but now performed in a much gentler, targeted and personalized manner.

The platform provides sufficient pressure output to release drugs into a specified neural circuit during awake behavior. The awake setup enables investigators to quantify the efficacy and duration of the neuromodulatory effects induced by specific neuromodulatory drugs, such as propofol[34] or ketamine. In addition, the behavioral readout can be used to assess the safety of the release at the functional level. For instance, damage of the LGN would result in profound degradation of the animal's visual discrimination ability[35,36].

Analogous protocols can be used to assess the efficacy and safety of cargo delivery across the blood-brain barrier (BBB)[21]. To achieve robust therapeutic effects, agents, such as chemotherapy, will likely need to be delivered across the BBB repeatedly and over multiple sessions. This may raise safety concerns[37]. Our reproducible targeting platform opens doors to systematic investigation of the effects of repeated ultrasound-based BBB opening.

Together, the platform described here provides the capacity to implement several, if not all, of the recent ultrasound-based approaches to targeted yet noninvasive brain intervention (Figure 5). The platform has the potential to bring these precision treatments to the millions of people with treatment-resistant neurological and psychiatric conditions, and is here made available for such applications.

Methods

Animals

One subject participated in this study (male *macaca mulatta*, age 6 years, weight 8 kg). The procedures were approved by the Institutional Animal Care and Use Committee of the University of Utah.

NHP Platform Positioning and Head Fixation

For the NHP experiments shown here, we developed an apparatus that ensures reproducible positioning of the platform with respect to the head from session to session, and at the same time allows us to head-fix NHPs and engage them in behavioral tasks. To achieve that, we developed a custom head frame that is attached to the skull via four titanium pins (Gray Matter Research, Bozeman, MT). Each pin is attached to the skull using three screws. The frame for the NHP experiments was designed in 3D cad software and produced with a 3D printer. A 3D drawing of the frame is available at `onetarget.us/software`. The frame is attached to a primate chair using two steel bars, mounted into the left and right side of the frame. Coupling of the transducer to the skull is achieved using a 6% polyvinyl alcohol (PVA) gel[38]. The subject's hair is shaved prior to each session. Shaving may not be necessary in the ultimate human

applications; the platform could detect the quality of the coupling and aberration due to the hair, and adjust the emitted ultrasound amplitude accordingly.

In each session, the system measures the accuracy of the device placement with respect to the head and the quality of the acoustic coupling using ultrasound imaging. Specifically, the system measures the distance between the transducer and the skull at six distinct locations. A pulse-echo measurement, performed on a 3x3 grid of elements, provides an estimate of the location of the skull relative to the transducer. The distance is measured by detecting the front edge of the reflected ultrasound energy and assuming a speed of sound of 1500 m/s in the coupling gel. The average difference in position relative to the position measured during MR thermometry was 0.47 ± 0.55 mm. The total power returned to each element (Figure 4, bottom) was $9 \pm 8\%$ lower across sessions compared to the power measured during the MR thermometry session.

MR Imaging

The system is fully MRI-compatible. Accurate targeting of specific deep brain regions can therefore be validated using MRI, such as MR thermometry or MR ARFI. We used MR thermometry. In this approach, a continuous, 5-second sonication is sufficient to increase temperature at the focal spot by about 2°C, enabling visualization of the focus without inducing long-term changes in the neural tissue.

All scans were performed using a 3T MRI scanner (Trio, Siemens Medical Solutions, Erlangen, Germany) with a 4-channel flex coil wrapped underneath the animal's head. High resolution 3D T1-weighted images were used for anatomical imaging and target identification; Magnetization Prepared Rapid Acquisition Gradient Echo (MPRAGE), TR=1900 ms, TE=3.39 ms, TI-900 ms, BW=180 Hz/pixel, flip angle 9°, FOV = 192x192x120 mm, resolution 1x1x1 mm, acquisition time 5:12 min. MR thermometry was performed with a 3D gradient recalled segmented echo planar imaging pulse sequence; TR=24 ms, TE=11 ms, BW=592 Hz/pixel, flip angle 12°, echo train length = 5 with monopolar readout, FOV = 144x117x36 mm, resolution 1.5x1.5x3.0 mm, acquisition time 4.6 s per dynamic image.

Registration of ultrasound and MR space was performed using three fiducial markers. After registration, the average euclidean distance between the estimated and the actual location of of the three fiducials (as measured by the 3-dimensional center of mass) was 2.5 mm. The transducer caused distortion along the subject's inferior/superior axis resulting in approximately 4 mm of error in the transducers registration in that dimension. The registration of the transducer to the subject's anatomy guided initial steering of the acoustic beam. Once the first thermometry signal was acquired, adjustments to the focal location were based primarily on the location of the thermometry signal, thus correcting any errors introduced by poor transducer localization.

It is well established that preferential absorption of ultrasound in the skull can lead to undesirable off-target heating. Indeed, clinical ablation trials rely on both a large transducer aperture and constant cooling of the scalp to mitigate this risk[26]. With a smaller transducer aperture and in the absence of active cooling investigators must assume that the temperature rise in the skull could be higher than at focus. Care should thus be taken to monitor the health of the skull and scalp between the transducer and the target when MR thermometry is used to validate acoustic targeting.

At the short durations used for neuromodulation in this study, heating of the skull was not a concern. The subject, who was awake, showed no signs of discomfort in response to the ultrasound.

Acoustic Intensity at Target

The MRI thermometry additionally allowed us to compute the ultrasound pressure delivered in the target. Assuming negligible conduction and perfusion and a continuous sonication, the acoustic intensity, I, is

related to the temperature rise, ΔT, by[39]

$$I = \frac{\rho C \Delta T}{\Delta t \alpha}, \tag{1}$$

where ρ, C, and α are the density, specific heat capacity, and acoustic absorption of the tissue and Δt is the time in which the temperature increase occurs. To minimize the effects of conduction and perfusion ΔT is chosen to be the maximum temperature measured in the seventh dynamic (the first dynamic in which the ultrasound is on). The center of k-space is acquired 2.3 seconds into each acquisition. Thus, Δt was set to 2.3 s. We assumed a density of 1046 kg/m^3, a specific heat capacity of 3630 J/K, and an acoustic absorption of 3.9 Np/m.

Stimulation Parameters

Our custom, 256 element transducer (Doppler Electronic Technologies, Guangzhou, China) can produce focal pressures greater than 3 MPa at its 650 kHz center frequency. The transducer geometry is semicircular, with a radius of curvature of 65 mm (see Figure 1). The elements are 4 x 4 mm square and the distance between elements is 4.2 mm. All stimuli used 650 kHz. The pulsed stimulus (10% duty) used a 500 Hz pulse repetition frequency. The peak focal pressure (estimated from the thermometry data) was 770 and 650 kPa in the right and left LGN respectively. The half power beam width for the right LGN was 1, 3.75, and 3.75 mm in the left/right, anterior/posterior, and superior/inferior dimensions, respectively. Using the same input voltage, the free field pressure–measured using a hydrophone–is 2.4 MPa at the location of the left and right LGN. Thus, the MR thermometry measurements suggest that about 30% of the pressure reaches the target through the individual layers. It is worth noting, nonetheless, that this estimate likely underestimates the actual pressure at target. In particular, the temperature measured by the MR is averaged spatially (across a voxel) and temporally (across the acquisition time); the actual peak temperature is thus higher than the measured average. In addition, a portion of the energy is distributed to the thermal conduction and vascular convection.

Task

We trained one NHP to perform a visual choice task. This task was used in many previous studies (e.g.,[10,40]). Briefly, the subject was seated in a comfortable primate chair and was presented with visual stimuli shown on a monitor. The subject's eye movements were tracked and recorded using an infrared eye tracker (Eyelink, SR Research, Ottowa, Canada). In the task, the subject first fixates a central target. Following its offset, one target appears on the left and one target on the right side of the screen. There is a brief, controllable delay between the onset of the two targets, which can range from -40 to 40 ms. We varied the location of the targets within 2.5 visual degrees to circumvent adaptation. The sonication of the left and right LGN was randomly interspersed with trials in which no ultrasound was delivered. In an ultrasound trial, a 300 ms stimulus was delivered 150 ms before the fixation point offset. The subject receives a liquid reward if he looks at the target that appeared first within 2 s. In the key condition in which both targets appear at the same time and during which we quantify the effect of ultrasound, the subject is rewarded for either choice.

Software

We designed custom software to integrate ultrasound sonication with both the MR thermometry and the behavioral task. The software can register the transducer to an MR coordinate system, output the targeted focus in both transducer and MR coordinates, and overlay the temperature change (as measured by MR thermometry) on the anatomy image. To protect the subject's scalp, skull, and neural tissue we used very

small temperature increases to visualize the focal spot. Thus, to improve the visualization, we included a noise reduction algorithm in our visualization software. The algorithm assumes an exponential increase in temperature during the sonication and an exponential decay in temperature after the ultrasound turns off. Voxels in which the temperature does not follow such a trend are ignored.

Similarly, we developed software that integrates a behavioral task with flexible sonication of the targeted neural circuit. The ultrasound controller accepts target coordinates and intensities from the server running the behavioral task. Synchronization of the sonication with presentation of the visual stimulus is achieved with a TTL pulse. All of the ultrasound software was developed within the Verasonics framework and is available at `onetarget.us/software`.

Acknowledgments

This development of the platform and its application in NHPs was supported by the National Institute of Neurological Disorders and Stroke, Grants 5R00NS100986 and F32MH123019. We thank Tyler Davis and Eric Burdett for facilitating this work.

References

1. Lancet. Life, death, and disability in 2016. *The Lancet* **390**, 1084–1423 (2017).
2. Ahrnsbrak, R., Bose, J., Hedden, S., Lipari, R. & Park-Lee, E. Key substance use and mental health indicators in the United States: Results from the 2016 National Survey on Drug Use and Health. *Cent. for Behav. Heal. Stat. Qual. Subst. Abus. Mental Heal. Serv. Adm. Rockville, MD, USA* (2017).
3. Bystritsky, A. Treatment-resistant anxiety disorders. *Mol. psychiatry* **11**, 805–814 (2006).
4. Al-Harbi, K. S. Treatment-resistant depression: therapeutic trends, challenges, and future directions. *Patient preference adherence* **6**, 369 (2012).
5. Zesiewicz, T. A., Chari, A., Jahan, I., Miller, A. M. & Sullivan, K. L. Overview of essential tremor. *Neuropsychiatr. disease treatment* **6**, 401 (2010).
6. Elias, W. J. *et al.* A randomized trial of focused ultrasound thalamotomy for essential tremor. *New Engl. J. Medicine* **375**, 730–739 (2016).
7. Ferguson, J. M. Ssri antidepressant medications: adverse effects and tolerability. *Prim. care companion to J. clinical psychiatry* **3**, 22 (2001).
8. Karceski, S. C. Seizure medications and their side effects. *Neurology* **69**, E27–E29 (2007).
9. Fry, W. J. Use of intense ultrasound in neurological research. *Am. journal physical medicine* **37**, 143–7 (1958).
10. Kubanek, J. *et al.* Remote, brain region–specific control of choice behavior with ultrasonic waves. *Sci. Adv.* **6**, eaaz4193, DOI: 10.1126/sciadv.aaz4193 (2020).
11. Deffieux, T., Younan, Y., Wattiez, N., Tanter, M. & Pouget, P. Low-Intensity Focused Ultrasound Modulates Monkey Visuomotor Behavior. *Curr. Biol.* **23**, 2430–2433, DOI: 10.1016/j.cub.2013.10.029 (2013).
12. Tufail, Y. *et al.* Transcranial Pulsed Ultrasound Stimulates Intact Brain Circuits. *Neuron* **66**, 681–694, DOI: 10.1016/j.neuron.2010.05.008 (2010).
13. Lee, W. *et al.* Image-Guided Transcranial Focused Ultrasound Stimulates Human Primary Somatosensory Cortex. *Sci. Reports* **5**, 8743, DOI: 10.1038/srep08743 (2015).

14. Legon, W. *et al.* Transcranial focused ultrasound modulates the activity of primary somatosensory cortex in humans. *Nat. neuroscience* **17**, 322–329, DOI: 10.1038/nn.3620 (2014).

15. Verhagen, L. *et al.* Offline impact of transcranial focused ultrasound on cortical activation in primates. *eLife* **8**, 1–28, DOI: 10.7554/elife.40541 (2019).

16. Folloni, D. *et al.* Manipulation of subcortical and deep cortical activity in the primate brain using transcranial focused ultrasound stimulation. *Neuron* **101**, 1109–1116 (2019).

17. Bongioanni, A. *et al.* Activation and disruption of a neural mechanism for novel choice in monkeys. *Nature* 1–5 (2021).

18. Wang, J. B., Aryal, M., Zhong, Q., Vyas, D. B. & Airan, R. D. Noninvasive Ultrasonic Drug Uncaging Maps Whole-Brain Functional Networks. *Neuron* **100**, 728–738.e7, DOI: 10.1016/j.neuron.2018.10.042 (2018).

19. Rapoport, N. *et al.* Ultrasound-mediated tumor imaging and nanotherapy using drug loaded, block copolymer stabilized perfluorocarbon nanoemulsions. *J. Control. Release* **153**, 4–15, DOI: 10.1016/j.jconrel.2011.01.022 (2011).

20. Lea-Banks, H., O'Reilly, M. A., Hamani, C. & Hynynen, K. Localized anesthesia of a specific brain region using ultrasound-responsive barbiturate nanodroplets. *Theranostics* **10**, 2849–2858, DOI: 10.7150/thno.41566 (2020).

21. Abrahao, A. *et al.* First-in-human trial of blood–brain barrier opening in amyotrophic lateral sclerosis using MR-guided focused ultrasound. *Nat. Commun.* **10**, 1–9, DOI: 10.1038/s41467-019-12426-9 (2019).

22. Braun, U. *et al.* From maps to multi-dimensional network mechanisms of mental disorders. *Neuron* **97**, 14–31 (2018).

23. Price, J. L. & Drevets, W. C. Neural circuits underlying the pathophysiology of mood disorders. *Trends cognitive sciences* **16**, 61–71 (2012).

24. Peirs, C. & Seal, R. P. Neural circuits for pain: recent advances and current views. *Science* **354**, 578–584 (2016).

25. Insel, T. R. & Cuthbert, B. N. Brain disorders? Precisely. *Science* **348**, 499–500 (2015).

26. Ghanouni, P. *et al.* Transcranial MRI-guided focused ultrasound: A review of the technologic and neurologic applications. *Am. J. Roentgenol.* **205**, 150–159, DOI: 10.2214/AJR.14.13632 (2015).

27. Guo, H. *et al.* Ultrasound produces extensive brain activation via a cochlear pathway. *Neuron* (2018).

28. Sato, T., Shapiro, M. G. & Tsao, D. Y. Ultrasonic Neuromodulation Causes Widespread Cortical Activation via an Indirect Auditory Mechanism. *Neuron* **98**, 1031–1041.e5, DOI: 10.1016/j.neuron.2018.05.009 (2018).

29. Plaksin, M., Kimmel, E. & Shoham, S. Cell-Type-Selective Effects of Intramembrane Cavitation as a Unifying Theoretical Framework for Ultrasonic Neuromodulation. *eNeuro* **3**, DOI: 10.1523/ENEURO.0136-15.2016 (2016).

30. Tyler, W. J., Lani, S. W. & Hwang, G. M. Ultrasonic modulation of neural circuit activity. *Curr. opinion neurobiology* **50**, 222–231 (2018).

31. Kubanek, J. Neuromodulation with transcranial focused ultrasound. *Neurosurg. Focus.* **44**, E14 (2018).

32. Naor, O., Krupa, S. & Shoham, S. Ultrasonic neuromodulation. *J. Neural Eng.* **13**, 031003 (2016).

33. Fomenko, A. *et al.* Systematic examination of low-intensity ultrasound parameters on human motor cortex excitability and behavior. *Elife* **9**, e54497 (2020).

34. Wang, J. B., Aryal, M., Zhong, Q., Vyas, D. B. & Airan, R. D. Noninvasive ultrasonic drug uncaging maps whole-brain functional networks. *Neuron* **100**, 728–738 (2018).

35. Ro, T., Rorden, C., Driver, J. & Rafal, R. Ipsilesional biases in saccades but not perception after lesions of the human inferior parietal lobule. *J. Cogn. Neurosci.* **13**, 920–929 (2001).

36. Schiller, P. H. & Tehovnik, E. J. Cortical inhibitory circuits in eye-movement generation. *Eur. J. Neurosci.* **18**, 3127–3133 (2003).

37. Kovacs, Z. I. *et al.* Disrupting the blood–brain barrier by focused ultrasound induces sterile inflammation. *Proc. Natl. Acad. Sci.* **114**, E75–E84, DOI: 10.1073/pnas.1614777114 (2017).

38. Lee, W., Lee, S. D., Park, M. Y., Yang, J. & Yoo, S.-S. Evaluation of polyvinyl alcohol cryogel as an acoustic coupling medium for low-intensity transcranial focused ultrasound. *Int. J. Imaging Syst. Technol.* **24**, 332–338, DOI: 10.1002/ima.22110 (2014).

39. Pennes, H. H. Analysis of Tissue and Arterial Blood Temperatures in the Resting Human Forearm. *J. Appl. Physiol.* **1**, 93–122, DOI: 10.1152/jappl.1948.1.2.93 (1948).

40. Kubanek, J., Li, J. M. & Snyder, L. H. Motor role of parietal cortex in a monkey model of hemispatial neglect. *Proc. Natl. Acad. Sci. United States Am.* **112**, E2067–E2072, DOI: 10.1073/pnas.1418324112 (2015).

Supplemental Material

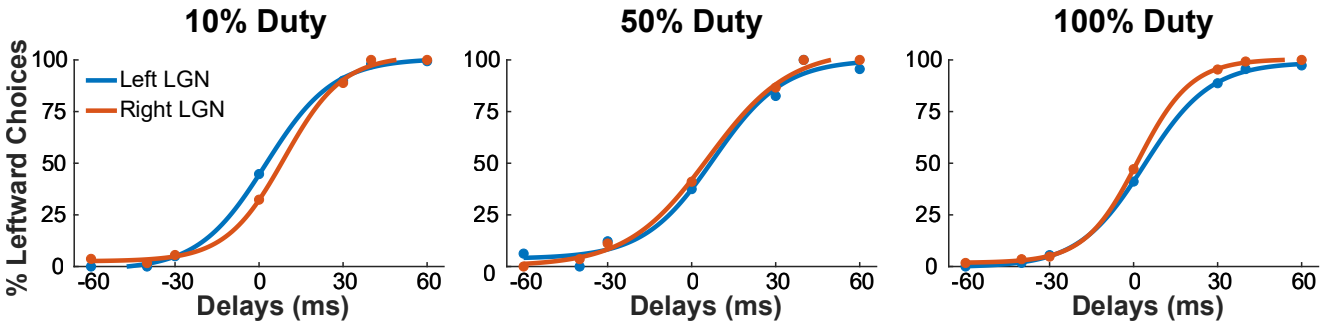

Figure 1. Behavioral Bias is Mediated by Sonicated Target and Stimulus Type.
Relative to sonication of the right LGN, sonication of the left LGN induces a leftward bias for a 10% duty stimulus and a rightward bias for a 50 and 100% duty stimulus.